Formation of Orientation-Ordered Superlattices of Magnetite Magnetic Nanocrystals from Shape-Segregated Self-Assemblies†

Qing Song,‡,⊥ Yong Ding,§,⊥ Zhong Lin Wang,*,§ and Z. John Zhang*,‡

School of Chemistry and Biochemistry, Georgia Institute of Technology, Atlanta, Georgia 30332-0400, and School of Materials Science and Engineering, Georgia Institute of Technology, Atlanta, Georgia 30332-0245

Received: August 15, 2006; In Final Form: October 11, 2006

Magnetic magnetite (Fe_3O_4) nanocrystals have been synthesized by combining nonhydrolytic reaction with seed-mediated growth. The shape of these magnetite nanocrystals can be controlled either as pure spheres or a mixture of mainly faceted nanocrystals. Faceted magnetite nanocrystals consist of truncated tetrahedral platelets (TTPs), truncated octahedrons (TOs), and octahedrons (OTs). Transmission electron microscopy analysis indicates that the faceted nanocrystal mixture tends to self-segregate based upon the shape in a self-assembly process, and each shape forms its own distinct crystallographic orientation-ordered superlattice assemblies. Self-assemblies of the Fe_3O_4 nanocrystals in the shapes of TTP, TO, and OT show hexagonal, primitive cubic, and distorted body-centered cubic (bcc) superlattice structures, respectively. The possible mechanism for the formation of different superstructures is attributed to van der Waals interactions. Nanocrystals with different shapes provide diverse building blocks for bottom-up approaches in building nano- and mesosystems. Furthermore, the self-segregation phenomenon of different shaped nanocrystals in self-assembly processes could be very important in envisioning efficient assembly strategies for nanoscience- and nanotechnology-based devices.

Introduction

Nanomaterials have inspired broad interests in various areas for both their size- and shape-dependent properties and for a variety of technological applications.[1,2] Enormous progress has been made in producing metal and semiconductor nanocrystals with various shapes such as rods, multiple-branched rods, nanocubes, nanodisks and nanoprisms.[3−14] However, the shape-controlled synthesis of metal oxides in the nanometer regime has limited success, especially for magnetic metal oxides, even though such materials are of great importance in a variety of technological applications ranging from biomedical areas to magnetic data storage.[15−18] Moreover, it is also of great fundamental and practical interest to prepare monolayers, thin films and superstructures by using nanocrystals as building blocks to explore the novel collective optical, electrical, and magnetic phenomena possessed by nanosystems.[19,20]

Recent research has demonstrated a wide variety of self-assemblies built by metallic, semiconductor and other compound nanocrystals.[21−24] It is interesting to note that iron oxide nanocrystals were among the first observed superstructures.[25] Although orientation ordering has been observed in a short range in the assembly of Ag, Au, and Co spherical nanocrystals,[26−28] long-range orientation ordering in general is limited, although translational symmetry could be achieved perfectly. It seems easier for faceted nanocrystals to form orientation-ordered self-assembly. For instance, metallic FePt nanocubes can self-assemble into an array with a (100) oriented texture.[29] The preservation of orientation ordering could place high restrictive requirements on the size, size distribution, and shape of the nanocrystals. Self-assembly of nanocrystals tends to follow a general rule of surface-to-surface, thus it is very likely that orientation ordering is easily lost if the particles are spherical.

The synthesis of magnetic iron oxide nanocrystals has long been of keen interest in magnetic data storage, biological application, drug delivery, and ferrofluids.[30−33] Recent synthesis studies on magnetite nanocrystals have mainly focused on size control,[34−37] while relatively few results on shape control have been reported.[38−40] In this work, we present the synthesis of Fe_3O_4 nanocrystals with controllable size and a certain degree of shape control. Three typical shapes are reported, including truncated tetrahedral platelet (TTP), truncated octahedron (TO), and octahedron (OT). The Fe_3O_4 nanocrystals of different shapes are shape-selectively self-segregated from each other to form orientation-ordered superstructures through a self-assembly process. Fe_3O_4 nanocrystals in shapes of TTP, TO, and OT show hexagonal, primitive cubic-like, and distorted body-centered cubic (bcc) superlattice structures, respectively.

Experimental

Synthesis of Spherical Fe_3O_4 Nanocrystals as Seeds. The synthesis includes two steps: the spherical seed formation and seed-mediated growth. The reactions were taken place under N_2 protection. Ethanol, hexane, and acetone from Fisher Scientific, Inc. were used as received. Phenyl ether (99%), oleic acid (90%), oleylamine (tech. 70%), iron (III) acetylacetonate (Fe(III)$(acac)_3$) (97%), 1,2-hexadecandiol, and 1-octadecanol were purchased from Aldrich Chemical Co. and used without further treatment. In the seed-formation step, a mixture of 30 mL of phenyl ether, 2 mmol of Fe(III)$(acac)_3$, 10 mmol of 1,2-hexadecandiol, 3 mL of oleic acid, and 3 mL of oleylamine was quickly heated up to 260 °C, kept reflux for 30 min at that

† Part of the special issue "Arthur J. Nozik Festschrift".

* Corresponding authors. E-mail: zhang@gatech.edu (Z.J.Z.); zhong.wang@mse.gatech.edu (Z.L.W.).

‡ School of Chemistry and Biochemistry.

§ School of Materials Science and Engineering.

⊥ These authors have contributed equally to this work.

10.1021/jp0652695 CCC: $33.50
Published on Web 12/14/2006

temperature, and then cooled to room temperature. After adding ethanol, a black precipitate could be collected by either centrifugation or using a permanent magnet. After washing twice with ethanol, the precipitate was redispersed in hexane. The size of produced Fe_3O_4 nanocrystals is about 4 nm. To make larger Fe_3O_4 nanocrystals, seed-mediated growth was applied. For example, after combining 60 mg of 8 nm seeds with 1 mmol of Fe(III)$(acac)_3$, 5 mmol of 1-octadecanol, 3 mL of oleic acid, and 3 mL of oleylamine in 30 mL of phenyl ether, 10 nm Fe_3O_4 nanocrystals were formed. The shape of the nanocrystals is mainly spherical under such reaction conditions.

Synthesis of Faceted Fe_3O_4 Nanocrystals. Spherical Fe_3O_4 nanocrystals of different sizes were used as seeds, and the procedure was similar to that of making spherical ones except for the reaction temperature. For example, a solution containing 60 mg of 10 nm seeds and 2 mmol of Fe(III)$(acac)_3$ was mixed with 30 mL of phenyl ether, 10 mmol of 1-octadecanol, 3 mL of oleic acid, and 3 mL of oleylamine, and was heated up to 220 °C over a period of 2 h. The solution was then kept reflux for 30 min before being allowed to cool to room temperature. The shapes of the Fe_3O_4 nanocrystals obtained in such reaction conditions were mainly TTP, TO, and OT with sizes of about 12−14 nm.

Characterization. Powder X-ray diffraction patterns were recorded using a Bruker D8 Advance diffractometer with Cu Kα irradiation ($\lambda = 1.54056$ Å). Transmission electron microscopy (TEM) investigations were carried out using a JEM 100C under 100 kV and a JEM 4000EX under 400 kV. The samples for TEM analysis were prepared by dispersing a drop of nanocrystal suspension on amorphous carbon-coated copper grids. The carrier solvent was hexane mixed with 0.2% (v/v) oleic acid.

Results and Discussion

Magnetic magnetite (Fe_3O_4) nanocrystals have been synthesized by combining nonhydrolytic reaction with seed-mediated growth. Spherical nanocrystals were initially synthesized. The as-studied nanocrystals were prepared by using seed-mediated growth with 4 nm spherical nanoparticles as the seeds. The shape of these magnetite nanocrystals can be controlled either as pure spheres or a mixture of mainly faceted nanocrystals. Faceted magnetite nanocrystals consist of TTPs, TOs, and OTs. The studies from powder X-ray diffraction showed that the spherical and faceted nanocrystals are consistent with the spinel structure of magnetite. Chemical elemental analysis using the inductively coupled plasma atomic emission spectroscopy (ICP-AES) method also confirmed the chemical composition as being magnetite. Magnetic characterization has shown the spherical and faceted magnetite nanocrystals possessing typical superparamagnetic features at room temperature.

The shape control of these magnetite nanocrystals was achieved during the seed-mediated growth process by controlling the growth rate. Upon promoting a relatively faster growth through quickly raising the temperature of seed-mediated growth at 260 °C, most of the grown Fe_3O_4 nanocrystals are spherical. The faceted Fe_3O_4 nanocrystals are predominately formed if the growth rate is lowered by maintaining the growth temperature at 220 °C and, at the same time, keeping all other reaction parameters the same as the growth of spherical nanocrystals. Such distinct results strongly imply that there is a strong correlation between the shape evolution and the growth rates in the seed-mediated growth process. In the cubic spinel structure, the surface energy associated with {100}, {110}, and {111} facets are the lowest.[41−42] When the nanocrystal growth is slow at a relatively low temperature, the discrepancy of surface energy on different facets starts to play a dominant role in shape evolution. The areas of the lowest energy surface tend to be maximized, resulting in the growth of the nanocrystals with polyhedral shapes. When a faster growth rate occurred at a relatively higher temperature, a more homogeneous growth on all crystallographic directions became favorable, which leads to the formation of spherical-like particles.

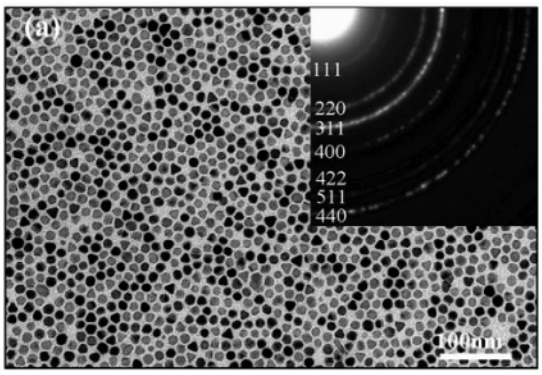

Figure 1. Monolayer of Fe_3O_4 nanocrystals. The inserted ring-patterned SAED clearly reveals that the orientations of the nanocrystals are random.

The self-assembly of magnetite nanocrystals was performed by evaporating a carrier solvent of hexane from a nanocrystal suspension with various concentrations. A typical TEM image of monolayer self-assembled Fe_3O_4 nanocrystals is shown in Figure 1, which was produced by using a low-concentration (∼0.1 mg/mL) suspension of faceted nanocrystals. The observed shapes of Fe_3O_4 nanocrystals are mainly TTP, TO, and OT. Although there is no uniform size across board due to the mixture nature of different shapes, the sizes of nanocrystals range from 12 to 14 nm and are approximately uniform for the nanocrystals with the same shape. The selected-area electron diffraction (SAED) pattern recorded from the region is inserted in Figure 1, which confirms the cubic spinel structure of the Fe_3O_4 nanocrystals. The ring features of the SAED pattern indicate the random orientations of these self-assembled nanocrystals.

With controlled evaporation of the carrier solvent from a hexane suspension of a higher nanocrystal concentration (∼3 mg/mL), the resulted self-assembly of faceted nanocrystals possesses multilayer structures (Figures 2, 3, and 4). Significantly, the different shaped Fe_3O_4 nanocrystals have gone through a shape-selected self-separation process and have formed three distinct superstructures with highly crystallographic orientation-ordered textures. Each superlattice is a self-assembly of the same shaped Fe_3O_4 nanocrystals. Figure 2a is the superstructure that has been self-assembled by the TTP-shaped Fe_3O_4 nanocrystals. The inserted high-magnification image shows the building blocks taking the shape of TTP and having a uniform size distribution. The interesting result is that the SAED pattern from the self-assembled nanocrystals in Figure 2b shows the single-crystal type [111] zone-axis pattern, which clearly indicates the orientation ordering among the nanocrystals in the self-assembly. The high-resolution TEM (HRTEM) image of a single TTP nanocrystal is shown in Figure 2c. The clear lattice image indicates that the nanocrystal is well crystallized. The truncated tetrahedral shape can be easily distinguished from the dark-field image inserted in Figure 2d, which shows uniform contrast across its width, indicating uniform thickness. The model of a TTP nanocrystal is inserted between panels c and d of Figure 2: two {111} planes served as the top/bottom surfaces,

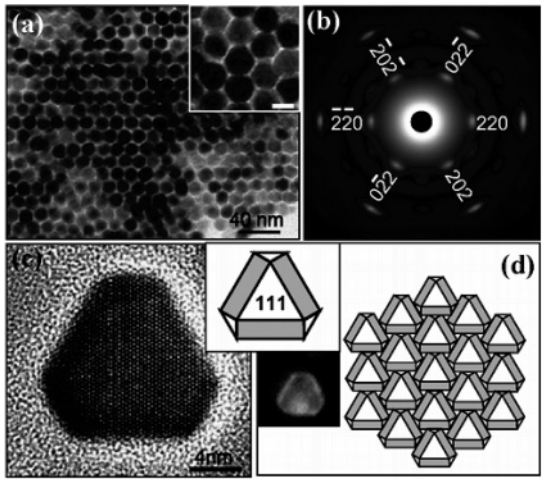

Figure 2. (a) Low- and high-magnification TEM images showing the hexagonal columnar superstructure built up by the TTP Fe_3O_4 nanocrystals. The scale bar for the inset is 10 nm. (b) SAED pattern of the superlattice. (c) HRTEM image of a single TTP nanocrystal. The inserted model between panels c and d shows the shape of the nanocrystal. (d) Top-view model of the superstructure. The inset is the dark-field image of a TTP nanocrystal.

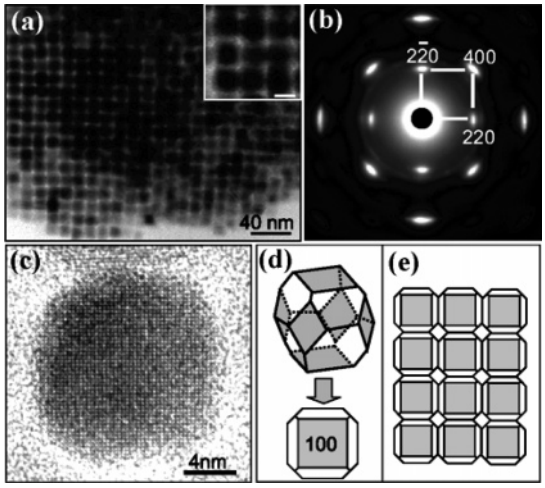

Figure 3. (a) Low- and high-magnification TEM images showing the primitive cubic-like superstructure assembled by the TO Fe_3O_4 nanocrystals. The scale bar for the inset is 10 nm. (b) SAED pattern of the superlattice. (c) HRTEM image of a single TO nanocrystal. (d) Three-dimensional model and two-dimensional projection of the nanocrystal. (e) Top-view model of the superstructure.

and six intersected {111} and {100} planes composed the side surfaces. Using the model as a building block, the self-assembled superstructure is sketched in Figure 2d. The TTP nanocrystals in plane tend to pack as close as possible. While in the perpendicular direction, the second plane tends to overlap right on the bottom plane without translation. Consequently, the holes in the multilayer area are clearly visible, and a superlattice with a hexagonal columnar structure is formed.

The superstructure built from self-assembled Fe_3O_4 nanocrystals with a TO shape is shown in Figure 3a. A high-magnification image from the multilayer area is inserted in Figure 3a. The corresponding SAED pattern is displayed in Figure 3b. This self-assembly is also orientation-ordered along the crystallographic zone axis. The electron beam of the SAED pattern is parallel to the [001] direction. The HRTEM image of a single TO nanocrystal is shown in Figure 3c; the four edges correspond to {220} planes. A three-dimensional model and a two-dimensional projection of the TO Fe_3O_4 nanocrystals are

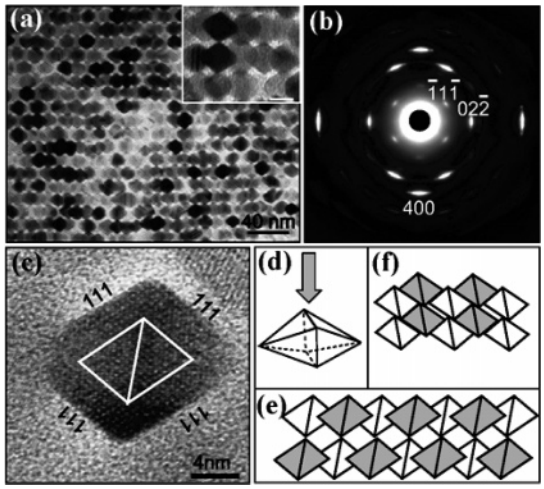

Figure 4. (a) Low- and high-magnification TEM images showing the bcc superstructure formed by the octahedral Fe_3O_4 nanocrystals. The scale bar for the inset is 10 nm. (b) SAED pattern of the superlattice. (c) HRTEM image of a single octahedral nanocrystal. (d) Three-dimensional model of the nanocrystal. (e,f) Top-view and side-view models of the superstructure, respectively.

illustrated in Figure 3d. The self-assembled superstructure built by the TO nanocrystals is sketched in Figure 3e. The second layer overlapped on the first layer without translation or twist, forming a simple cubic-like superstructure.

The image in Figure 4a displays the superstructure built up by the OT nanocrystals. From the inserted image, the overlap among the octahedral can be clearly observed. The SAED pattern in Figure 4b indicates that most of the building blocks take the same crystal orientation of [110]. The HRTEM image of a single nanocrystal in Figure 4c shows a well-faceted structure; the low contrast of the two horizontal corners is consistent with the projected thickness of the OT. The three-dimensional model is depicted in Figure 4d. Top-view and side-view illustrations of the self-assembled superstructure are sketched in Figure 4e,f, respectively. The self-assembly can be approximated to be a distorted bcc superstructure.

Clearly, the type of crystal structure of these observed superstructures and their specific crystallographic orientations depend upon the shapes of the Fe_3O_4 nanocrystal building blocks. Such results unambiguously demonstrate that the shape of nanocrystals plays a crucial role in self-assembly for determining both the crystal structure and the orientation of three-dimensional superstructures. There are two striking features in the formation of these superstructures. First, all self-assembled superstructures are the result of shape-selective self-segregation. Second, the contact in the packing sequence follows the face-to-face (facet-to-facet) mode between neighboring individual nanocrystals in all three types of superstructures. Certainly, it can be speculated that such oriented superstructure formation essentially originates from the energy balance between van der Waals attractive potential and repulsive potential among nanocrystals as well as between nanocrystals and the substrate. If considering nanocrystals with different shapes as "unlike molecules" and nanocrystals with the same type of shape as "like molecules", the shape-selective self-segregation assembly of different shaped nanocrystals should be a spontaneous process, which follows the usual consequence of an effective attraction between like molecules in a multicomponent mixture, providing that the interactions are not dominated by Coulombic or H-bonding forces.[43] In other words, such a shape-selective self-segregation process is the display in the nanomaterial regime

of the principle of the "like-dissolving-like" rule commonly encountered in molecular chemistry.

Furthermore, for faceted nanocrystals, theoretical studies have pointed out that the crystallographic orientation is mainly determined by the maximization of the van der Waals interactions between the facets of neighboring nanocrystals.[44−46] The face-to-face stacking mode gives rise to stronger van der Waals interactions than those of either edge-to-edge or corner-to-corner packing. The energy of attractive van der Waals interactions for face-to-face stocking is inversely proportional to the square of the distance between two faces, whereas, for edge-to-edge stacking, such a van der Waals interaction energy is inversely proportional to the separation distance.[47] Consequently, the face-to-face stacking sequence is favorable for maximizing the van der Waals attractive interactions among closely packed nanocrystals at shorter distances. The Fe_3O_4 nanocrystals in the studied size range are superparamagnetic and possess weak magnetic features.[48] The possible magnetic interactions are considered to play negligible roles in these self-assembly processes.

Conclusions

Magnetite nanocrystals with TTP, TO, and OT shapes have been synthesized by a seed-mediated growth method. The growth temperature is the key factor in controlling the shape of the Fe_3O_4 nanocrystals. Highly oriented three-dimensional superstructures built from such faceted Fe_3O_4 nanocrystals have been determined to be hexagonal, primitive cubic-like, and distorted bcc. The crystallographic orientations of superstructures are strongly related to the shapes of Fe_3O_4 nanocrystals. The face-to-face stacking mode in these superstructures is considered to be the result of maximizing van der Waals interaction energy. Nanocrystals with different shapes provide diverse building blocks for bottom-up approaches in building nano- and meso-systems. Furthermore, the self-segregation phenomenon of different shaped nanocrystals in self-assembly processes could be very important in envisioning efficient assembly strategies for nanoscience- and nanotechnology-based devices.

Acknowledgment. This work was supported in part by Sandia National Laboratory and the PECASE program. All TEM studies were performed at the Electron Microscopy Center at the Georgia Institute of Technology.

References and Notes

(1) Alivisatos, A. P. *Science* **1996**, *271*, 933.
(2) Heath, J. R. *Acc. Chem. Res.* **1999**, *32*, 388.
(3) Ahmadi, T. S.; Wang, Z. L.; Green, T. C.; Henglein, A.; El-Sayed, M. A. *Science* **1996**, *272*, 1924.
(4) Peng, X.; Manna, U.; Yang, W.; Wickham, J.; Scher, E.; Kadavanich, A.; Allvisatos, A. P. *Nature* **2000**, *404*, 59.
(5) Jin, R.; Cao, Y.; Mirkin, C. A.; Kelly, K. L.; Schatz, G. C.; Zheng, J. G. *Science* **2001**, *294*, 1901.
(6) Puntes, V. F.; Krishnan, K. M.; Alivisatos, A. P. *Science* **2001**, *291*, 2115.
(7) Manna, L.; Scher, E. C.; Alivisatos, A. P. *J. Am. Chem. Soc.* **2000**, *122*, 12700.
(8) Puntes, V. F.; Zanchet, D.; Erdonmez, C. K.; Alivisatos, A. P. *J. Am. Chem. Soc.* **2002**, *124*, 12874.
(9) Peng, Z. A.; Peng, X. *J. Am. Chem. Soc.* **2002**, *124*, 3343.
(10) Lee, S.-M.; Jun, Y.-w.; Cho, S.-N.; Cheon, J. *J. Am. Chem. Soc.* **2002**, *124*, 11244.
(11) Lisiecki, I. *J. Phys. Chem. B* **2005**, *109*, 12231.
(12) Norimatsu, F. Y.; Mizokoshi, Y.; Mori, K.; Mizugaki, T.; Ebitani, K.; Kaneda, K. *Chem. Lett.* **2006**, *35*, 276.
(13) Kumar, S.; Nann, T. *Small* **2006**, *2*, 316.
(14) Cheng, Y.; Wang, Y.; Bao, F.; Chen, D. *J. Phys. Chem. B* **2006**, *110*, 9448.
(15) Mitchell, D. G. *Magn. Reson. Imaging* **1997**, *7*, 1.
(16) Rety, F.; Clement, O.; Siauve, N.; Cuenod, C. A.; Carnot, F.; Sich, M.; Buisine, A.; Frija, G. *Magn. Reson. Imaging* **2000**, *12*, 734.
(17) Sugimoto, M. *J. Am. Ceram. Soc.* **1999**, *82*, 269.
(18) Pankhurst, Q. A.; Connolly, J.; Jones, S. K.; Dobson, J. *J. Phys. D: Appl. Phys.* **2003**, *36*, R167.
(19) Collier, C. P.; Vossmeyer, T.; Heath, J. R. *Annu. Rev. Phys. Chem.* **1998**, *49*, 371.
(20) Murray, C. B.; Kagan, C. R.; Bawendi, M. G. *Annu. Rev. Mater. Sci.* **2000**, *30*, 545.
(21) Murray, C. B.; Kagan, C. R.; Bawendi, M. G. *Science* **1995**, *270*, 1335.
(22) Sun, S.; Murray, C. B.; Weller, D.; Folks, L.; Moser, A. *Science* **2000**, *287*, 1989.
(23) Redl, F. X.; Cho, K. S.; Murray, C. B.; O'Brien, S. *Nature* **2003**, *423*, 968.
(24) Lisiecki, I.; Albouy, P.-A.; Pileni, M.-P. *Adv. Mater.* **2003**, *15*, 712.
(25) Bentzon, M. D.; Van, Wonterghem, J.; Moerup, S.; Tholen, A.; Koch, C. J. W. *Philos. Mag. B* **1989**, *60*, 169.
(26) Harfenist, S. A.; Wang, Z. L.; Alvarez, M. M.; Vezmar, I.; Whetten, R. L. *J. Phys. Chem.* **1996**, *100*, 13904.
(27) Wang, Z. L. *Adv. Mater.* **1998**, *10*, 13.
(28) Wang, Z. L.; Dai, Z.; Sun, S. *Adv. Mater.* **2000**, *12*, 1944.
(29) Chen, M.; Kim, J.; Liu, J. P.; Fan, H.; Sun, S. *J. Am. Chem. Soc.* **2006**, *128*, 7132.
(30) Cornell, R. M. *The Iron Oxides: Structure, Properties, Reactions, Occurrence and Uses*; VHC: Weinheim, Germany, 1996.
(31) Häfeli, U., Schütt, W.; Teller, J.; Zborowski, M. *Scientific and Clinical Applications of Magnetic Carriers*; Plenum Press: New York, 1997.
(32) Papisov, M. I.; Bogdanov, A., Jr.; Schaffer, B.; Nossiff, N.; Shen, T.; Weissleder, R.; Brady, T. J. *J. Magn. Magn. Mater.* **1993**, *122*, 383.
(33) Raj, K.; Moskowitz, B.; Casciari, R. *J. Magn. Magn. Mater.* **1995**, *149*, 174.
(34) Rockenberger, J.; Scher, E. C.; Alivisatos, A. P. *J. Am. Chem. Soc.* **1999**, *121*, 11595.
(35) Hyeon, T.; Lee, S. S.; Park, J.; Chung, Y.; Na, H. B. *J. Am. Chem. Soc.* **2001**, *123*, 12798.
(36) Sun, S.; Zeng, H. *J. Am. Chem. Soc.* **2002**, *124*, 8204.
(37) Sun, S.; Zeng, H.; Robinson, D. B.; Raoux, S.; Rice, P. M.; Wang, S. X.; Li, G. *J. Am. Chem. Soc.* **2004**, *126*, 273.
(38) Cheon, J.; Kang, N.-J.; Lee, S.-M.; Lee, J.-H.; Yoon, J.-H.; Oh, S. J. *J. Am. Chem. Soc.* **2004**, *126*, 1950.
(39) Song, Q.; Zhang, Z. J. *J. Am. Chem. Soc.* **2004**, *126*, 6164.
(40) Zeng, H.; Rice, P. M.; Wang, S. X.; Sun, S. *J. Am. Chem. Soc.* **2004**, *126*, 11458.
(41) Davies, M. J.; Parker, S. C.; Watson, G. W. *J. Mater. Chem.* **1994**, *4*, 813.
(42) Fang, C. M.; Parker, S. C.; De, With, G. *J. Am. Ceram. Soc.* **2000**, *83*, 2082.
(43) Israelachvili, J. N. *Intermolecular and Surface Forces*, 2nd ed.; Academic Press: New York, 1992.
(44) Ohara, P. C.; Leff, D. V.; Heath, J. R.; Gelbart, W. M. *Phys. Rev. Lett.* **1995**, *75*, 3466.
(45) Luedtke, W. D.; Landman, U. *J. Phys. Chem.* **1996**, *100*, 13323.
(46) Korgel, B. A.; Fullam, S.; Connolly, S.; Fitzmaurice, D. *J. Phys. Chem. B* **1998**, *102*, 8379.
(47) Hamaker, H. C. *Physica IV* **1937**, *4*, 1058.
(48) Song, Q.; Zhang, Z. J. *J. Phys. Chem. B* **2006**, *110*, 11205.